Electronic Supplementary Material (ESI) for Physical Chemistry Chemical Physics.


**Electronic Supplementary Information to accompany:**

# Multi-mass velocity map imaging study of the 805 nm strong field ionization of $CF_3I$.

Stuart W Crane,[a,#] Jason W L Lee [b,c] and Michael N R Ashfold [a]

[a] School of Chemistry, University of Bristol, Bristol, U.K. BS8 1TS

[b] Department of Chemistry, University of Oxford, Oxford, U.K. OX1 3TA

[c] Deutsches Elektronen Synchrotron DESY, Hamburg, Germany

[#] Current address:

Department of Chemistry, Brown University, Providence, RI 02912, U.S.A.

**Table S1**

Enthalpies of formation for $CF_3I$ and various of its possible fragmentation products, from ref. 1.

| $\Delta_f H$ (0 K) / kJ mol$^{-1}$ | | | | | |
|---|---|---|---|---|---|
| $CF_3I$ | −583.7 | | $CF_3I^+$ | | |
| $CF_3$ | −465.1 | | $CF_3^+$ | 409.3 | |
| $^1CF_2$ | −193.9 | | $CF_2^+$ | 908.1 | |
| $^3CF_2$ | 43.3 | | | | |
| CF | 243.2 | | $CF^+$ | 1122.9 | |
| C | 711.4 | | $C^+$ | 1797.9 | |
| $F(^2P_{3/2})$ | 77.3 | | $F^+$ | 1758.3 | |
| $F(^2P_{1/2})$ | 82.1 | | | | |
| $I(^2P_{3/2})$ | 107.2 | | $I^+$ | 1115.6 | |
| $I(^2P_{1/2})$ | 198.1 | | | | |

[1] B. Ruscic and D.H. Bross, Active Thermochemical Tables (ATcT) Values based on ver. 1.122r of the Thermochemical Network (2021); available at Active Thermochemical Tables - Thermochemical Data (anl.gov).

**Table S2**

Threshold energies for the processes: $CF_3I \rightarrow e^- + Y$, given $D_0(CF_3–I)$ = 225.8 kJ mol$^{-1}$ (2.34 eV),[1] a value consistent with results of previous photofragment translational spectroscopy studies.[2]

| Y | E / kJ mol$^{-1}$ | *E* / eV | Comment |
|---|---|---|---|
| $CF_3I^+$ | 1000.7 | 10.37 | |
| $CF_3^+ + I$ | 1099.2 | 11.39 | [3] |
| $CF_3 + I^+$ | 1234.2 | 12.80 | |
| $CF_2I^+ + F$ | | 13.4 | [4] |
| $CF_2^+ + F + I$ | 1675.3 | 17.36 | |
| $CF^+ + 2F + I$ | 1968.4 | 20.39 | |
| $CF_3^+ + I^+$ | 2108.6 | 21.84 | |
| $CF_2^+ + F + I^+$ | 2684.7 | 27.81 | |
| $CF_2I^+ + F^+$ | | 30.8 | |
| $CF_2^+ + F^+ + I$ | 3357.3 | 34.78 | |
| | | | |
| $CF_3I^{2+}$ | | 28.0 | [5] |
| $CF_3 + I^{2+}$ | | 31.94 | [6] |
| $CF_3^{2+} + I$ | | ~38 | [7] |
| $CF_3^{2+} + I^+$ | | ~48.5 | [7] |
| $CF_3^{2+} + I^{2+}$ | | ~68 | [6,7] |
| $CF_3^{2+} + I^{3+}$ | | ~97 | [6] |
| $CF_3^{2+} + I^{4+}$ | | ~137.5 | [6,7] |
| | | | |
| C + 3F + I | 1634.2 | 16.93 | [1] |
| $C^+ + 3F^+ + I^+$ | 8772.1 | 90.87 | [1] |

[1] B. Ruscic and D.H. Bross, Active Thermochemical Tables (ATcT) Values based on ver. 1.122r of the Thermochemical Network (2021); available at Active Thermochemical Tables - Thermochemical Data (anl.gov).

[2] F. Aguirre and S.T. Pratt, *J. Chem. Phys.*, **118**, 1175 (2003).

[3] Consistent with observed threshold for this process reported in photoionization studies by R.L. Asher and B. Ruscic, *J. Chem. Phys.*, **106**, 210 (1997).

[4] Threshold value reported by I. Powis, O. Dutuit, M. Richard-Viard and P.M. Guyon, *J. Chem. Phys*., **92**, 1643 (1990).

[5] Vertical excitation value, reported by J.H.D. Eland, R. Feifel and M. Hochlaf, *J. Chem. Phys*., **128**, 234303 (2008).

[6] Using $IE(I \rightarrow I^+)$ = 10.45 eV, $IE(I \rightarrow I^{2+})$ = 29.58 eV, $IE(I \rightarrow I^{3+})$ = 59.15 eV and $IE(I \rightarrow I^{4+})$ = 99.5 eV, from A. Kramida, Yu. Ralchenko, J. Reader, and NIST ASD Team (2018) *NIST Atomic Spectra Database* (ver. 5.9), (Online), Available: https://physics.nist.gov/asd, [2022, January 6], National Institute of Standards and Technology, Gaithersburg, NM. DOI: https://doi.org/10.18434/T4W30F.

[7] Using calculated value for adiabatic IP for $CF_3^+ \rightarrow CF_3^{2+}$ = 26.8 eV reported in J. Hrušák, N. Sändik and W. Koch, *Int. J. Mass Spectrom.*, **185**, 701-706 (1999) in reasonable agreement with value estimated experimentally (26.3 eV) in C.J. Proctor, C.J. Porter, T. Ast and J.H. Beynon, *Int. J. Mass Spectrom. Ion. Phys*., **41**, 251-263 (1982).

**Table S3**

Summary of *Z*-dependent fragmentation channels for $CF_3I^{Z+}$ ions identified in the present study.

| *Z* | Products | Process number |
|---|---|---|
| 1 | $CF_3^+ + I$ | (1) |
| | $CF_3 + I^+$ | (2) |
| | $CF_2I^+ + F$ | (3) |
| | | |
| 2 | $CF_3^+ + I^+$ | (4) |
| | $CF_{3-n}^+ + I^+ + nF$ (n = 1-3) | (4) + (5) |
| | $CF_2I^+ + F^+$ | (6) |
| | $CF_2^+ + IF^+$ | (7) |
| | $CF_2I^{2+} + F$ | (8) |
| | $CF_3 + I^{2+}$ | (9) |
| | | |
| 3 | $CF_3^+ + I^{2+}$ | (11) |
| | $CF_{3-n}^+ + I^{2+} + nF$ (n = 1-3) | (11) + (5) |
| | $CF_3^{2+} + I^+$ | (12) |
| | $CF_2I^{2+} + F^+$ | (13) |
| | | |
| 4 | $CF_3^{2+} + I^{2+}$ | (14) |
| | $CF_{3-n}^{2+} + I^{2+} + nF$ (n = 1-3) | (14) + (5) |
| | $CF^+ + I^{3+}$ | (17) |
| | | |
| 5 | $CF_3^{2+} + I^{3+}$ | (18) |
| | $\{CF_3^{3+}\} + I^{2+}$ | (19) * |
| | | |

* { } signifies expectation that the 4-atom $CF_3^{3+}$ species will have a very fleeting nature.

**Figure S1**

Comparisons of the $P(v)$ distributions of the $I^+$ and $CF_3^+$ fragment ions measured following SFI of $CF_3I$ with $\lambda$ = 805 nm photons at $I$ = 650 TW cm$^{-2}$ derived from the symmetrized 3-time bin images shown in fig. 2 and 4 (green), from the similarly symmetrized 1- (*i.e*. centre time bin only, red) and 7-time bin, blue) images, and from the central slice (violet) obtained by Abel inverting the symmetrized crushed 7-time bin images. For consistency, both sliced images were obtained by integrating over the range 5 $\leq \theta \leq$ 175°, to avoid the center-line noise.

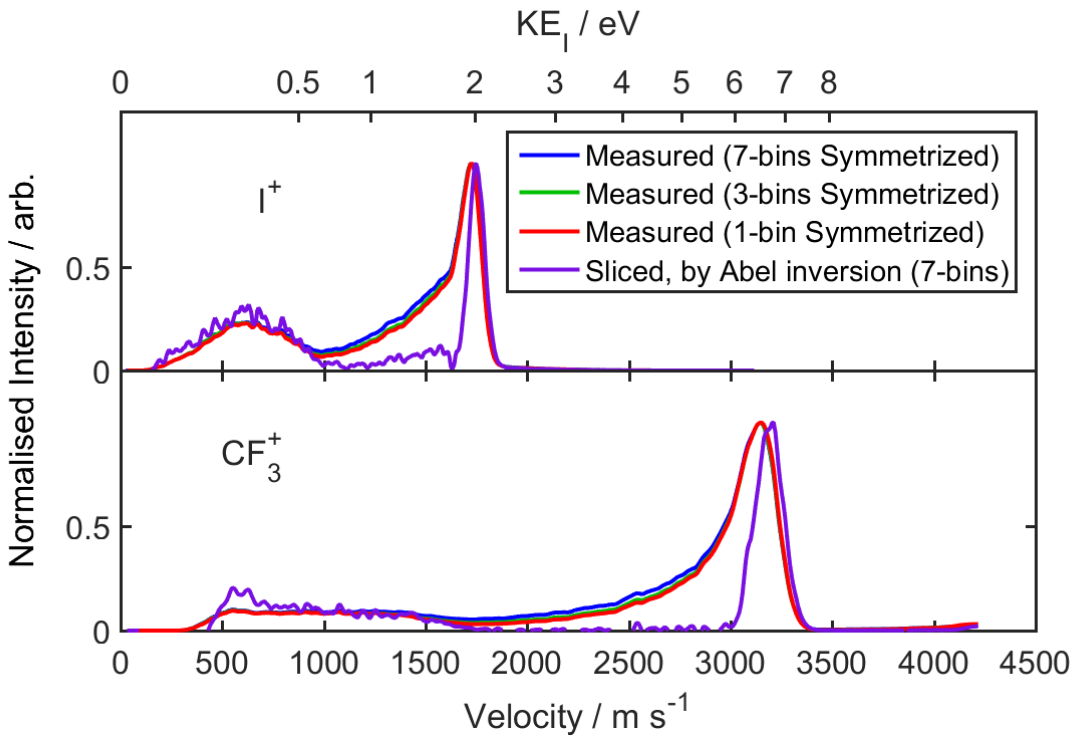

**Figure S2**

Symmetrized images of the (a) $F^+$ and (b) $F^{2+}$ fragments observed following SFI of $CF_3I$ with $\lambda$ = 805 nm photons at $I$ = 1300, 650 and 260 TW cm$^{-2}$, with the orientation of the $\boldsymbol{\varepsilon}$ vector of the SFI laser radiation shown by the double headed red arrow in the top left panel. The corresponding $P(v)$ distributions are shown in (c) with, in each case, the feature of greatest interest normalised to unit intensity. The corresponding $KE_F$ scale is shown on the top x-axis.

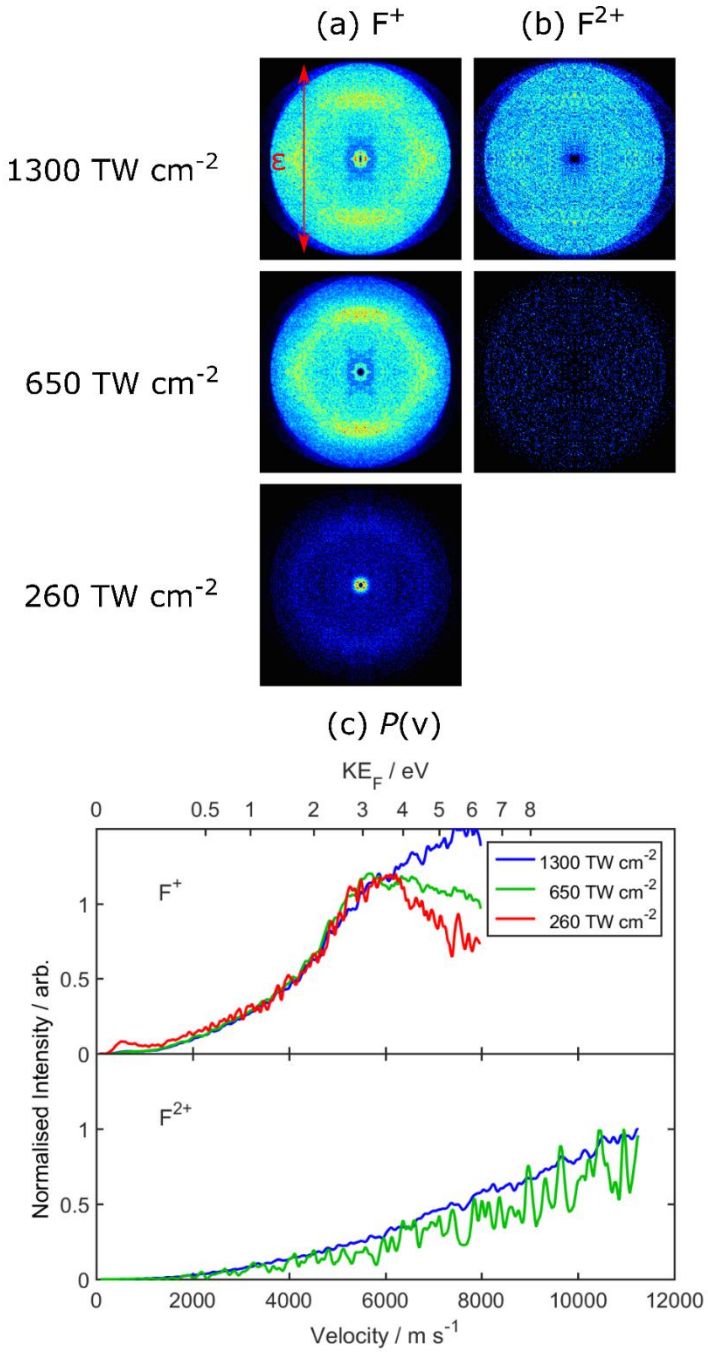

**Figure S3**

Symmetrized images of the (a) $CF_2I^+$ and (b) $IF^+$ fragments observed following SFI of $CF_3I$ with $\lambda$ = 805 nm photons at $I$ = 1300, 650 and 260 TW cm$^{-2}$, with the orientation of the $\boldsymbol{\varepsilon}$ vector of the SFI laser radiation shown by the double headed red arrow in the top left panel. The corresponding $P(v)$ distributions are shown in (c) with, in each case, the feature of greatest interest normalised to unit intensity. The lowest-velocity part of each $P(v)$ distribution is plotted in a fainter hue in recognition of the reduced sensitivity at the detector centre.

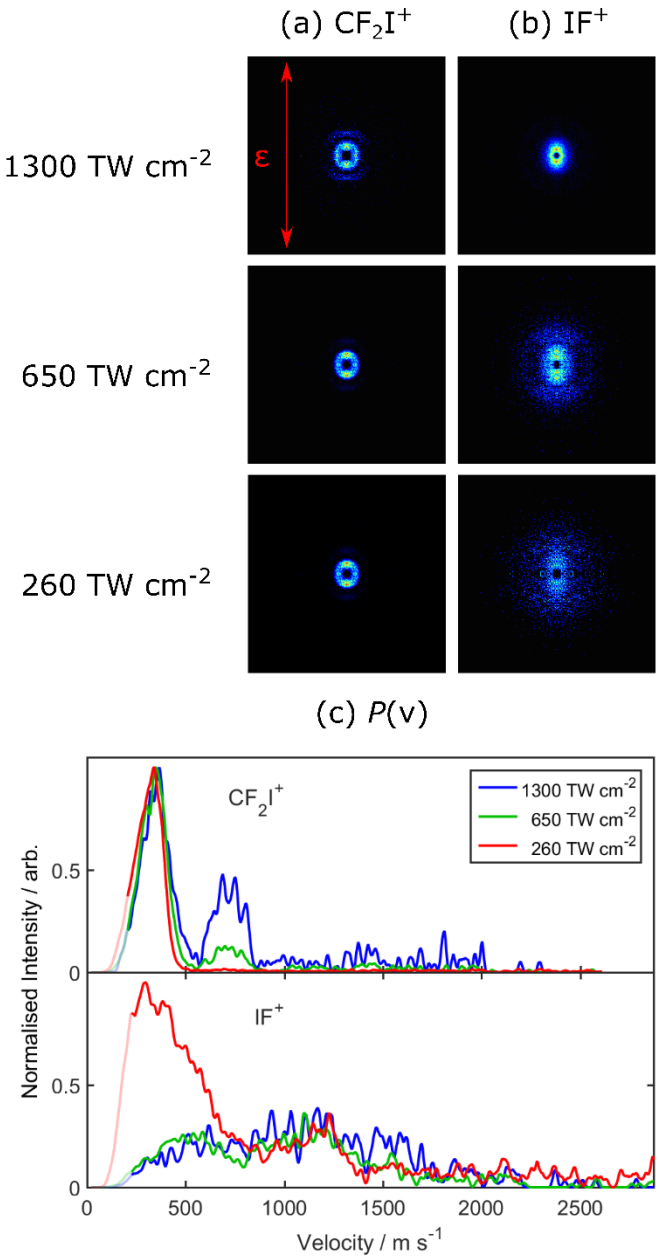

**Figure S4**

(a) Symmetrized images of the $CF_2I^{2+}$ fragments observed following SFI of $CF_3I$ with $\lambda$ = 805 nm photons at $I$ = 1300, 650 and 260 TW cm$^{-2}$, with the orientation of the $\boldsymbol{\varepsilon}$ vector of the SFI laser radiation shown by the double headed red arrow in the top left panel. The corresponding $P(v)$ distributions are shown in (b) with, in each case, the feature at low velocity normalised to unit intensity. The small peak at $v$ ~1050 m s$^{-1}$ is highlighted by an arrow, and the lowest- and highest-velocity parts of the various $P(v)$ distributions have been plotted in a fainter hue in recognition of, respectively, the reduced sensitivity at the detector centre, and the likelihood that signal from traces of bromothiophene contamination (from a preceding experiment) is responsible for the feature centred at $v$ ~2400 m s$^{-1}$ observed at $I$ = 1300 TW cm$^{-2}$.

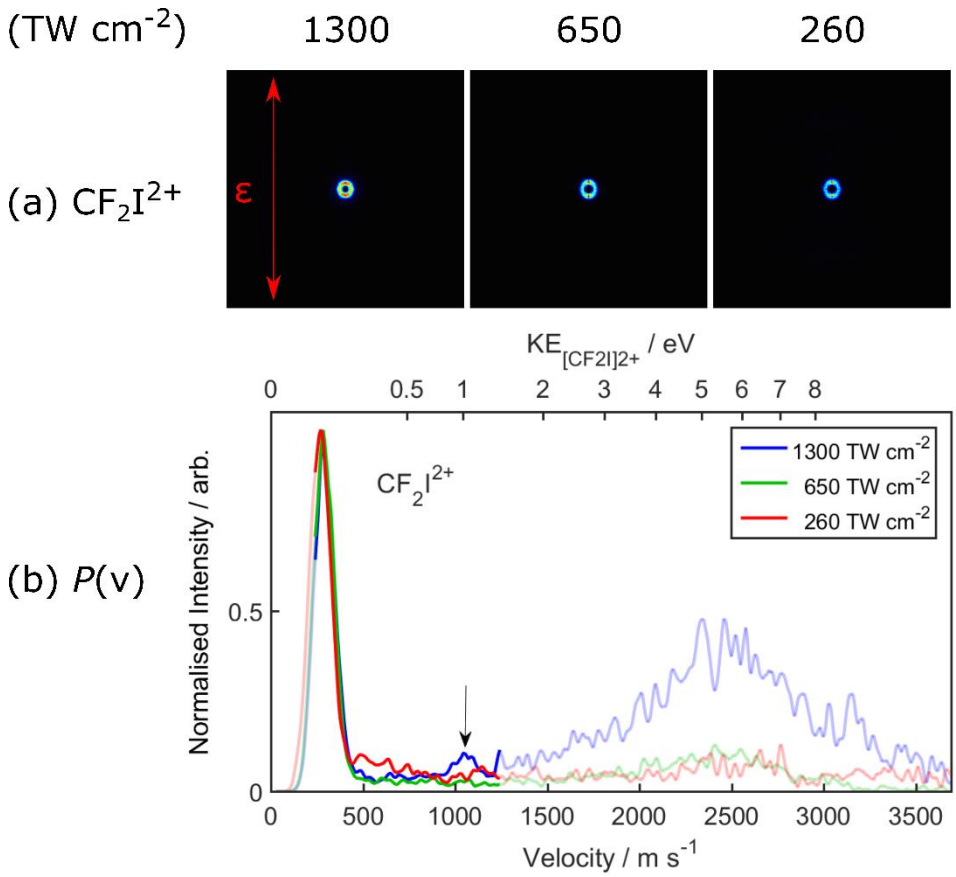

**Figure S5**

($I^{q+}$, $CF_3^+$), ($I^{q+}$, $CF_2^+$) and ($I^{q+}$, $CF^+$) ($q$ = 1, 2) covariance map images from the $I$ = 260 TW $cm^{-2}$ data from SFI of $CF_3I$ with, in each case, the recoil direction of the reference ion vertically upwards as illustrated by the red arrow in the top left-hand panel. The covariance signal of interest in each case is bounded by dashed white lines.

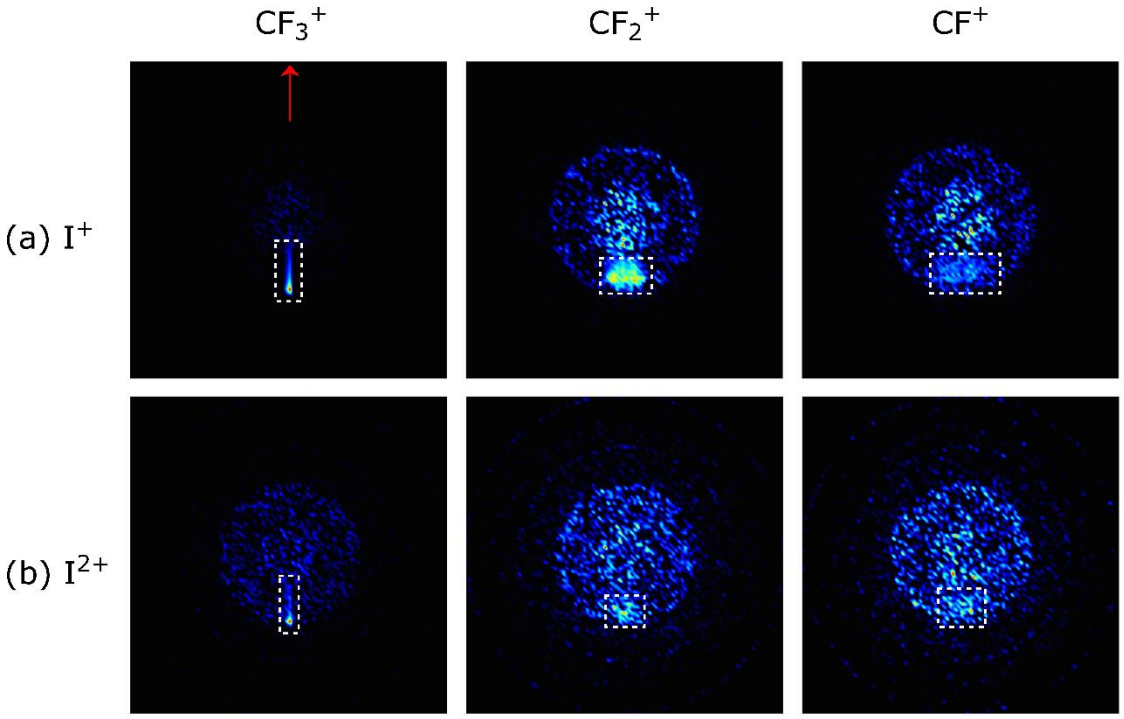

**Figure S6**

($I^{q+}$, $CF_3^+$ ($q$ = 1, 2)) and ($CF_3^+$, $I^{q+}$) covariance map images from the $I$ = 650 and 1300 TW cm$^{-2}$ data from SFI of $CF_3I$ with, in each case, the recoil direction of the reference ion vertically upwards as illustrated by the red arrow in the top left-hand panel. The covariance signal of interest, bounded by dashed white lines, is not identifiable in the ($I^{2+}$, $CF_3^+$) covariance map image from the $I$ = 1300 TW cm$^{-2}$ data.

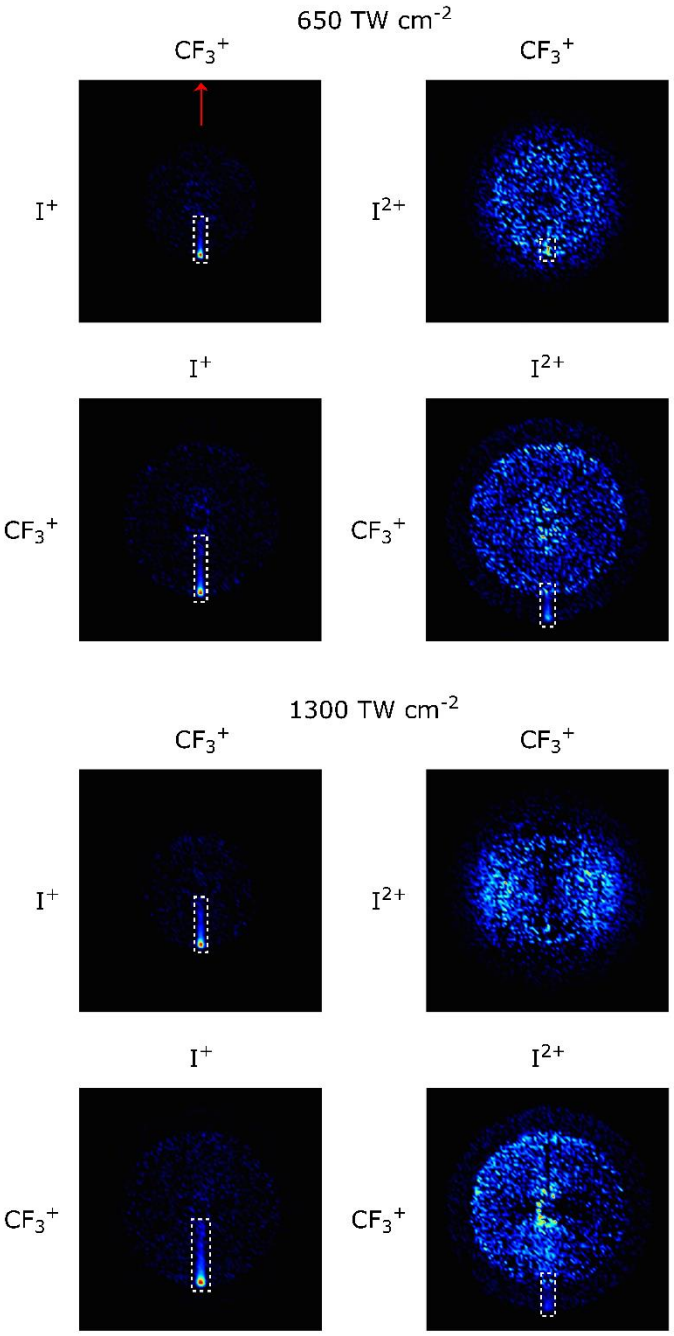

**Figure S7**

($I^{2+}$, $CF_3^{2+}$) and ($CF_3^{2+}$, $I^{2+}$) covariance map images from the $I$ = 650 TW cm$^{-2}$ data from SFI of $CF_3I$. In each case, the recoil direction of the reference ion is vertically upwards, as illustrated by the red arrow in the top left-hand panel. The covariance signal of interest in the left-hand image is bounded by dashed white lines.

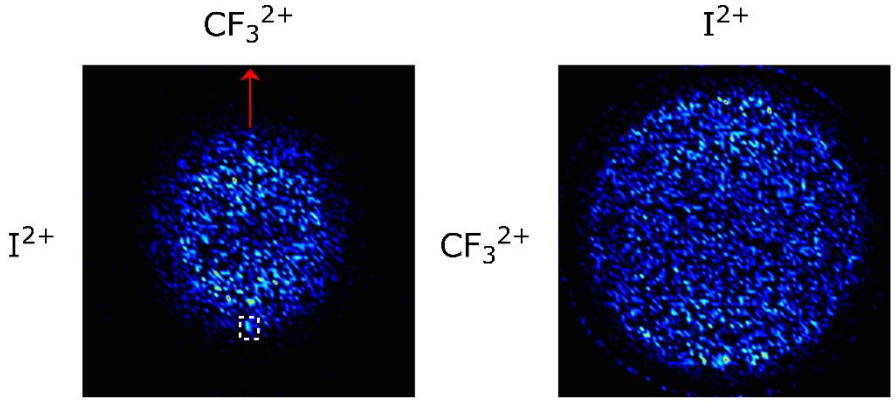

**Figure S8**

($IF^+$, $CF_2^+$) and ($CF_2I^+$, $F^+$) covariance map images from the $I$ = 260 TW $cm^{-2}$ data from SFI of $CF_3I$ with, in each case, the recoil direction of the reference ion vertically upwards as illustrated by the red arrow in the top left-hand panel. The covariance signal of interest in each case is bounded by dashed white lines.